

UC Berkeley

UC Berkeley Previously Published Works

Title

The diversity and evolution of microbial dissimilatory phosphite oxidation

Permalink

<https://escholarship.org/uc/item/7xv9v3nt>

Journal

Proceedings of the National Academy of Sciences of the United States of America, 118(11)

ISSN

0027-8424

Authors

Ewens, Sophia D
Gomberg, Alexa FS
Barnum, Tyler P
[et al.](#)

Publication Date

2021-03-16

DOI

10.1073/pnas.2020024118

Peer reviewed

1

2 **Main Manuscript for:**

3 **The Diversity and Evolution of Microbial Dissimilatory Phosphite Oxidation**

4 Sophia D. Ewens^{1,2}, Alexa F. S. Gomberg¹, Tyler P. Barnum¹, Mikayla A. Borton⁴,
5 Hans K. Carlson³, Kelly C. Wrighton⁴, John D. Coates^{1,2}

6

7 ¹Department of Plant and Microbial Biology, University of California, Berkeley, CA, USA

8 ²Energy & Biosciences Institute, University of California, Berkeley, CA, USA

9 ³Environmental Genomics and Systems Biology Division, Lawrence Berkeley National Lab,
10 Berkeley, CA, USA

11 ⁴Department of Soil and Crop Sciences, Colorado State University, Fort Collins, CO, USA

12

13 Corresponding Author: John D. Coates

14 Coates Laboratory, Koshland Hall, Room 241, University of California, Berkeley, Berkeley, CA
15 94720 | (510) 643-8455 | jdcoates@berkeley.edu

16

17 **ORCID:**

18 Kelly C. Wrighton: 0000-0003-0434-4217

19 Hans K. Carlson: 0000-0002-1583-5313

20 Alexa F. S. Gomberg: 0000-0002-3596-9191

21

22 **Classification**

23 Major: Biological Sciences

24 Minor: Microbiology

25

26 **Keywords**

27 reduced phosphorous, phosphite, phosphorus, energy metabolism, genome-resolved
28 metagenomics, ancient metabolism

29

30 **Author Contributions**

31 S.E., T.B., and J.C. conceived and planned metagenomic experimentation and analyses. S.E. and
32 J.C. conceived and planned wet-lab experiments. S.E., M.B., K.W., and J.C. conceived and
33 planned taxonomic and metabolic analyses. S.E. and M.B. performed taxonomic and metabolic
34 analyses. S.E. performed wet-lab experiments and metagenomic analyses. S.E. and A.G.
35 performed evolutionary analyses. S.E. wrote the manuscript. J.D. supervised the project. S.E.,
36 A.G., T.B., H.C., J.C. contributed to the interpretation of results. All authors provided critical
37 feedback and helped shape the research, analyses and manuscript.

38

39 **This PDF file includes:**

40 Main Text

41 Figures 1 to 7 are included separately

42 SI Figures S1 to S5 are included separately

43 SI Datasets S1 to S9 are included separately

44 SI Appendix Files S1 to S7 are included separately

45

46 **Abstract**

47 Phosphite is the most energetically favorable chemotrophic electron donor known, with a half-cell
48 potential (E°) of -650 mV for the $\text{PO}_4^{3-}/\text{PO}_3^{3-}$ couple. Since the discovery of microbial dissimilatory
49 phosphite oxidation (DPO) in 2000, the environmental distribution, evolution, and diversity of DPO
50 microorganisms (DPOM) has remained enigmatic and only two species have been identified. Here
51 metagenomic sequencing of phosphite enriched microbial communities enabled the genome
52 reconstruction and metabolic characterization of 21 novel DPOM. These DPOM spanned six
53 classes of bacteria, including the *Negativicutes*, *Desulfotomaculia*, *Synergistia*, *Syntrophia*,
54 *Desulfobacteria* and *Desulfomonilia_A*. Comparing the DPO genes from the genomes of enriched
55 organisms to over 17,000 publicly available metagenomes revealed the global existence of this
56 metabolism in diverse anoxic environments, including wastewaters, sediments, and subsurface
57 aquifers. Despite their newfound environmental and taxonomic diversity, metagenomic analyses
58 suggested that the typical DPOM is a chemolithoautotroph that occupies low-oxygen environments
59 and specializes in phosphite oxidation coupled to CO_2 reduction. Phylogenetic analyses indicated
60 that the DPO genes form a highly conserved cluster that likely has ancient origins predating the
61 split of monoderm and diderm bacteria. By coupling microbial cultivation strategies with
62 metagenomics, these studies highlighted the unsampled metabolic versatility latent in microbial
63 communities. We have uncovered the unexpected prevalence, diversity, biochemical
64 specialization, and ancient origins of a unique metabolism central to the redox cycling of
65 phosphorus, a primary nutrient on earth.

66 **Significance Statement**

67 Geochemical models of the phosphorus (P) cycle uniquely ignore microbial redox transformations.
68 Yet phosphite is a reduced P source that has been detected in several environments at
69 concentrations that suggest a contemporary P redox cycle. Microbial dissimilatory phosphite
70 oxidation (DPO) converts soluble phosphite into phosphate, and a false notion of rarity has limited
71 our understanding of its diversity and environmental distribution. Here we demonstrate that DPO is
72 an ancient energy metabolism hosted by taxonomically diverse, autotrophic bacteria that exist
73 globally throughout anoxic environments. DPO microorganisms are therefore likely to have
74 provided bioavailable phosphate and fixed carbon to anoxic ecosystems throughout Earth's history
75 and continue to do so in contemporary environments.

76
77 **Main Text**

78
79 **Introduction**

80 Phosphite (PO_3^{3-}) is a highly soluble, reduced compound that can account for over 30% of the total
81 dissolved inorganic phosphorus in diverse environments^{1,2}. Evidence suggests that meteorite
82 impacts deposited substantial phosphite quantities on early Earth, but its abiotic oxidation to
83 phosphate after the Great Oxidation Event (~2.5 billion years ago [Gya]) is assumed to have
84 rendered phosphite negligible in neoteric environments³. Surprisingly, phosphite has been detected
85 in diverse reducing environments, and up to 1 μM was observed in some surface waters,
86 suggesting contemporary neogenesis^{1,3}. Geothermal and hydrothermal systems may generate
87 phosphite through metal phosphide corrosion and iron-mediated phosphate reduction, and some
88 phosphite may be derived from biological phosphonate degradation or anomalous phosphate
89 reduction^{1,4,5}. Meanwhile, some phosphite accumulation is likely attributable to anthropogenic
90 activity because comparatively higher concentrations of phosphite have been identified in
91 contaminated environments and industrial wastewaters^{1,2,6}.

92
93 Despite its enigmatic distribution, functional gene presence in the IMG database² predicts that
94 phosphite is assimilated as a phosphorus source by approximately 1.5% of sequenced
95 microorganisms^{2,7-9}. However, the $\text{PO}_4^{3-}/\text{PO}_3^{3-}$ redox couple also has an extremely low potential
96 ($E^{\circ} = -650$ mV), and microorganisms can alternatively use phosphite as a sole electron donor and
97 energy source, excreting biogenic phosphate from cells¹⁰. With the low potential of the $\text{PO}_4^{3-}/\text{PO}_3^{3-}$
98 redox couple, phosphite represents the most energetically favorable chemotrophic microbial

99 electron donor described¹¹, yet only two DPOM have been cultured, and only one has been
100 isolated.

101
102 DPO was first identified in *Desulfotignum phosphitoxidans* strain FiPS-3, an autotrophic
103 homoacetogenic facultative sulfate-reducing bacterium, isolated from Venetian brackish
104 sediments¹². DPO in FiPS-3 is attributed to the *ptx-ptd* gene cluster (*ptxDE-ptdCFGHI*), which FiPS-
105 3 likely acquired through horizontal gene transfer (HGT)^{13–15}. FiPS-3's most closely related cultured
106 isolate is incapable of DPO although the organisms share 99% 16S rRNA gene identity¹⁶. The
107 second known DPOM, *Ca. Phosphitivorax anaerolimi* Phox-21, was enriched from wastewater
108 collected in Oakland, California, and recently, another *Phosphitivorax* strain (*Ca. P. anaerolimi* F81)
109 was identified in Danish wastewater^{17,18}. Phox-21 grows chemolithoautotrophically with phosphite
110 and carbon dioxide (CO₂) as the sole electron donor and acceptor, respectively, and is the first
111 naturally occurring species proposed to fix CO₂ via the reductive glycine pathway^{17,19,20}. The
112 reductive glycine pathway has since been confirmed to naturally fix CO₂ in wild-type *Desulfovibrio*
113 *desulfuricans*²¹. Phox-21 harbors all *ptx-ptd* genes, but unlike FiPS-3, lacks *ptdG* (a putative
114 transcriptional regulator) and shows no evidence of horizontal acquisition of the *ptx-ptd* cluster^{2,13}.
115 Understanding the evolutionary history of DPO metabolism is consequently limited by the existence
116 of only two characterized DPOM whose *ptx-ptd* clusters exhibit deviating patterns of composition
117 and inheritance.

118
119 Scarce representation also limits our understanding of the genes, organisms, and environments
120 that support DPO. It is difficult to predict the range of DPO taxa because *D. phosphitoxidans* FiPS-
121 3 and *Ca. P. anaerolimi* represent distinct taxonomic classes (*Desulfobacteria* and
122 *Desulfomonilia_A*), and their closest relatives are either uncultured or unable to catalyze DPO².
123 The environmental context of DPO remains ambiguous since DPOM have only been identified in
124 three distinct locations globally^{16–18}. Furthermore, the *ptx-ptd* cluster has unresolved genetic
125 diversity. *D. phosphitoxidans* FiPS-3 and *Ca. P. anaerolimi* species have *ptx-ptd* clusters with
126 alternative synteny and gene composition, and the PtxD proteins from FiPS-3 and Phox-21 share
127 only 55% amino acid sequence similarity¹⁷. Recognizing the breadth of hosts and environments
128 supporting this metabolism and characterizing the underlying biochemistry and genetics would
129 facilitate understanding of how DPOM impact the phosphorus cycle.

130 Here we present the selective enrichment of diverse DPOM in wastewater digester sludge from
131 facilities around the San Francisco Bay area. Metagenome-assembled genomes (MAGs)
132 uncovered 21 DPOM spanning three disparate phyla. Comparative genomics revealed
133 conservation of energy generation and carbon utilization pathways among DPOM genomes,
134 despite taxonomic diversity. We also identified DPO genes throughout global metagenome
135 databases and described the diversity of the *ptx-ptd* cluster. The phylogeny of *ptx-ptd* genes
136 suggests that DPO metabolism is vertically inherited as a conserved unit since before the split of
137 monoderm (Gram-positive) and diderm (Gram-negative) bacteria. Collectively, our results show
138 that DPO is widespread across diverse environments and bacterial taxa, and likely represents a
139 vestige of ancient microbial life.

140

141 Results

142

143 **Selective Enrichment.** We hypothesized that DPOM are cultivatable from wastewater sludge
144 because phosphite can represent up to 2.27% of total dissolved wastewater phosphorus²² and
145 because both strains of *Ca. P. anaerolimi* were identified in wastewater digester sludge^{17,18}.
146 Accordingly, sludge from six San Francisco Bay area facilities were used to inoculate 30 enrichment
147 cultures (SI Dataset S1). All cultures were grown in bicarbonate-buffered basal medium amended
148 with 10 mM phosphite and multivariate exogenous electron acceptors (CO₂-only, CO₂+SO₄²⁻, or
149 CO₂+NO₃⁻) (SI Dataset S1). Rumen fluid (5% by volume) was added to stimulate DPOM growth¹⁷.

150 Phosphite oxidation was observed in 26 of 30 enrichments and across all six wastewater facilities
151 (Fig. 1A & B, SI Dataset S1). When stationary phase enrichments were re-spiked with phosphite,
152 DPO activity resumed. No phosphite oxidation occurred in autoclaved controls (Fig. 1A). Based
153 on prior experience¹⁷, the high percentage of active DPO enrichments was unpredicted, indicating
154 a greater prevalence of DPOM than previously assumed.

155 **CO₂ Preference.** DPO was impacted by the amended electron-acceptor. Active enrichments with
156 only CO₂ supported the highest average phosphite oxidation rate (0.64±0.17 mM PO₃³⁻/day for CO₂
157 versus 0.56±0.10 and 0.50±0.20 mM PO₃³⁻/day for NO₃⁻ and SO₄²⁻, respectively). CO₂ also
158 supported DPO from all six sample sites. Despite the availability of nitrate and sulfate, neither
159 electron acceptor was definitively coupled to phosphite oxidation (Fig. 1C). While all amended
160 cultures consumed nitrate, it was metabolized before phosphite oxidation was complete,
161 suggesting utilization independent of DPO. In fact, when compared to other cultures with the same
162 inoculum, nitrate delayed or even excluded DPO (Fig. 1C). Meanwhile, although sulfate was
163 consistently consumed at the expected ratio, if reduced to sulfide coupled to phosphite oxidation
164 (1 mol sulfate per 4 mols phosphite), the timing of sulfate consumption was variable and frequently
165 offset from DPO (Fig. 1C). This suggests that sulfate reducers may be utilizing a reduced metabolite
166 from DPO activity. Consistent with this, both of the characterized DPOM either grow preferentially
167 (FiPS-3) or exclusively (Phox-21) by autotrophy and utilize CO₂ as an electron acceptor. In the
168 case of FiPS-3, the reduced carbon end-product is acetate¹⁶, which is readily utilized by sulfate
169 reducers. Our results support a DPOM preference for CO₂ and indicate that alternative electron
170 acceptors may inhibit DPO activity².

171 **DPOM Identification.** To characterize the active DPOM, we recovered metagenome-assembled
172 genomes (MAGs) from CO₂-only enrichments. To identify candidate DPOM, we searched all MAGs
173 using custom-built profile-HMMs (Appendix Files S1 – S7) for each of the seven *ptx-ptd* genes^{13,15}.
174 In total, 21 genomes had at least one gene from the *ptx-ptd* cluster (DPO MAGs), and of these, 19
175 were of high quality (>90% complete; <5% redundant) (SI Dataset S3)²⁴. DPO MAGs were enriched
176 in all phosphite amended communities (compared to no-phosphite controls) (Fig. 2A) and were
177 dominant in all but one community (SL1) (Fig. 2B). Furthermore, every sequenced community had
178 at least one DPO MAG (Fig. 2B). These results confirmed that DPO activity in phosphite amended
179 enrichments was dependent on the *ptx-ptd* genes and further indicates that these genes serve as
180 effective probes for DPOM.

181 **DPOM Taxonomy.** DPOM taxonomy assignments were made using (i) reconstructed 16S rRNA
182 gene fragments²⁵, (ii) multigene alignments using the genome taxonomy database (GTDB)²⁶, and
183 (iii) alignment of the ribosomal S8 proteins (rpS8)²⁷. Assignments were congruent in each instance
184 and visualized in Figure 3. Prior to our study, DPOM had been identified as belonging to only two
185 taxonomic classes of the *Desulfobacterota* phylum. In contrast, DPOM in our enrichments span the
186 monoderm-diderm taxonomic boundaries and include three phyla (*Desulfobacterota*, *Firmicutes*,
187 and *Synergistota*) and six classes (*Negativicutes*, *Desulfotomaculia*, *Synergistia*, *Syntrophia*,
188 *Desulfobacteria* and *Desulfomonilia_A*) (Fig. 3).

189 *Desulfomonilia_A* was the most sampled class of DPOM (Fig. 3), comprising 13 of 21 DPO MAGs.
190 They were enriched from all six sample sites and were present in nine communities. Furthermore,
191 they were the most relatively abundant DPO MAG (representing >85%) in each of eight
192 communities, indicating a possible advantage under our enrichment conditions (Figs. 2B, 3).
193 *Desulfomonilia_A* is an uncultured class that has recently been distinguished from the
194 *Desulfomonilia* (<https://gtdb.ecogenomic.org/>). Consistent with this, the *Desulfomonilia*
195 are represented by *Desulfomonile tiedjei*, which shares just 49% rpS8 sequence identity to the most
196 closely related DPO MAG of *Desulfomonilia_A*^{28,29} (Fig. 3). All DPO MAGs of the *Desulfomonilia_A*
197 class belong to the uncultured order UBA1062 (previously denoted GW-28)¹⁷, which includes Ca.
198 *Phosphitivorax* (SI Dataset S3). The monophyletic separation of the *Desulfomonilia_A* DPOM
199 supports the hypothesis that Ca. *Phosphitivorax* species are part of a unique order, and possibly a
200 unique class, for which DPO is a common metabolic feature¹⁷.

201 Beyond the *Desulfomonilia_A* DPOM, we recovered eight additional genomic representatives from
202 four novel classes (*Negativicutes*, *Desulfotomaculia*, *Synergistia*, and *Syntrophia*) (Fig. 3). While
203 most of these are minority DPOM in their respective communities, at least three (*Pelotomaculaceae*
204 SL1, Ca. *Smithella* SM1, and Ca. *Smithella* LM1) dominate their DPOM populations (>83%) (Figs.
205 2B, 3). The Ca. *Negativicutes* and Ca. *Desulfotomaculia* MAGs represent the first DPO genomes
206 taxonomically assigned to the *Firmicutes* phylum, highlighting the broad evolutionary divergence of
207 DPOM^{30,31}.

208 The closest cultured relatives of DPO MAGs share 57-95% rpS8 amino acid sequence identity (Fig.
209 3), which surpasses the species threshold (<98.3%)²⁷. Furthermore, multigene classification by
210 GTDB designates these related isolates as belonging to at least different genera²⁷, making
211 predictions about DPOM physiology from taxonomy unreliable. Regardless, all characterized DPO
212 MAG relatives, regardless of taxonomy, are obligately anaerobic chemoorganotrophs.
213 Furthermore, the *Desulfomonilia_A*, *Desulfotomaculia*, and *Syntrophia* classes contain canonical
214 representatives that are dependent on syntrophic associations^{18,31-34}. The phylogenetic
215 relatedness of our DPOM to notoriously fastidious syntrophic organisms could explain the difficulty
216 in isolating DPOM¹⁷.

217 The 16S rRNA gene is the canonical taxonomic marker for resolving microbial speciation. While
218 not present in all DPO MAGs, 86% (n=18) contained the 16S rRNA gene, enabling refined
219 taxonomic analyses (SI Dataset S4). To capture the novelty of enriched DPOM, we used EMIRGE
220 to reconstruct full-length 16S rRNA gene sequences that were BLAST searched in the SILVA
221 database^{25,35}. We determined that the DPOM represented 14 new strains, six new species, and
222 one new genus based on standardized relatedness metrics²⁷. Proposed names and etymologies
223 are provided in SI Dataset S4. The novel genus, represented by *Cosmobacter schinkii* SL3 (named
224 in recognition of Bernhard Schink, for his exemplary contributions to microbiology and discovery of
225 the first DPOM^{12,16}), is the second characterized genus of the *Desulfomonilia_A* UBA1062 order,
226 in addition to Ca. *Phosphitivorax*. Consequently, UBA1062 was expanded to include two genera
227 and five species (Fig. 3).

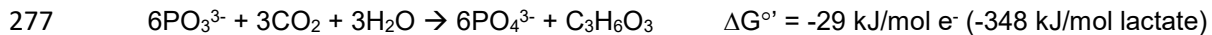
228 **Metabolic Traits.** The genomes of FiPS-3 and Phox-21 have been used to predict the mechanism
229 for DPO energy conservation^{13,17}. In the model (Fig. 4), the Ptx-Ptd protein cluster is hypothesized
230 to oxidize phosphite and generate NADH and ATP through substrate level phosphorylation.
231 Alternative reducing equivalents are likely produced via a Na⁺ motive force, ferredoxin, and an
232 electron confurcation mechanism. The model proposes CO₂ to be fixed into biomass via the
233 reductive glycine pathway, as was suggested for Phox-21¹⁷. In contrast, FiPS-3 utilizes the Wood-
234 Ljungdahl pathway¹³. By comparing the genomes of DPO MAGs to FiPS-3 and Phox-21, we found
235 highly conserved metabolic traits beyond the *ptx-ptd* gene cluster, regardless of taxonomy.

236 **Energy Conservation.** Like Phox-21, all DPO MAGs were missing a canonical membrane-bound
237 electron transport chain (ETC), as complexes II-IV were either absent or incomplete (Fig. 5).
238 *Sporomusaceae* SM1 of the *Negativicutes* class had a complete NADH-quinone oxidoreductase
239 (complex I), including the N, Q, and P-modules for NADH dehydrogenase activity, quinone
240 reduction, and proton translocation, respectively. However, all other DPO MAGs only contained N-
241 module subunits (Fig. 5, SI Dataset S5). The N-module houses the FMN and FeS clusters for
242 electron transport, as well as the NADH binding site. It also chimerically associates with other
243 protein complexes, such as formate dehydrogenases, catalyzing reversible NADH-dependent
244 formate production^{36,37}. Poehlein *et al.* suggested that the FiPS-3 N-module may directly transfer
245 electrons from NADH to ferredoxin¹³. However, direct NADH-dependent ferredoxin reduction is
246 thermodynamically unfavorable³⁸. Furthermore, the N-module of DPO MAGs is located in various
247 genomic contexts, making it unclear whether the commonality is uniquely associated with DPO
248 activity or with alternative cellular functions.

249 In Phox-21, ferredoxin reduction by NADH is attributed to a sodium translocating ferredoxin:NADH
250 oxidoreductase (Rnf) driven by a Na⁺ motive force¹⁷ (Fig. 4). Consistent with Phox-21, an Rnf

251 complex was present in the *Synergistia* and nearly all *Desulfomonilia_A* DPO MAGs (Fig. 5). In
252 contrast, the Rnf was absent from the *Negativicutes*, *Desulfotomaculia*, and *Syntrophia* DPO
253 MAGs, suggesting that it is dispensable or replaceable for DPO activity. The ion motive force for
254 Rnf activity in Phox-21 is likely provided by a cation-translocating F-type ATPase at the expense of
255 ATP (Fig. 4). The F-type ATPase was present in every DPO MAG, except one (*Synergistaceae*
256 SL3) which had the V-type (Fig. 5). While two genomes (*Syntrophales* LM1 and *Pelotomaculaceae*
257 LM1) were missing several ATPase subunits, these were only 61% and 69% complete (SI Dataset
258 S3)²⁴. Given the universal absence of an ETC in DPO MAGs, the ATPases are likely involved in
259 ATP hydrolysis with the concomitant generation of a cation motive force.

260 **CO₂ as an Electron Acceptor.** No DPO MAGs harbored functional pathways for methanogenesis
261 or common respiratory pathways (oxygen, nitrate, or sulfate), which is similar to Phox-21 and
262 consistent with the absence of ETC complexes (SI Fig. S2). Furthermore, CO₂ was the only
263 exogenous electron acceptor available to DPOM in sequenced cultures. Consistent with Phox-21¹⁷,
264 a physiological survey of one of our enrichments showed that CO₂ was necessary and sufficient to
265 support phosphite oxidation and growth (Fig. 6). As observed in Phox-21, comparative genomics
266 of DPO MAGs revealed a notable absence of any canonical CO₂-reduction pathways (Fig. 5). While
267 FiPS-3 can use CO₂ as an electron acceptor by reducing it to acetate via the Wood-Ljungdahl
268 pathway¹⁶, carbon reduction in Phox-21 was attributed to the reductive glycine pathway¹⁷. This is
269 comprised of the methyl branch of the Wood-Ljungdahl pathway, combined with the glycine
270 cleavage system, serine hydroxymethyltransferase, and serine deaminase to produce pyruvate as
271 an anabolic intermediate^{17,21} (Fig. 4). The Phox-21 final product of CO₂ reduction remains
272 enigmatic, as the genes for pyruvate conversion to acetate (phosphotransacetylase and acetate
273 kinase) are missing from the genome. Lactate is a possibility, as the genomes of Phox-21 and all
274 other *Desulfomonilia_A* DPO MAGs contain D-lactate dehydrogenase, which converts pyruvate to
275 lactate at the expense of NADH (Fig. 4). This is an energetically favorable reaction that accounts
276 for all reducing equivalents produced via phosphite oxidation according to figure 4 and:



278 **CO₂ Fixation to Biomass.** In addition to serving as the electron acceptor for DPOM, CO₂ is also
279 fixed into biomass as the carbon source¹⁷ (Fig. 6). While none of the DPO MAGs contained any
280 canonical CO₂ fixation pathways³⁹, twelve in the *Desulfomonilia_A*, *Negativicutes*, and *Syntrophia*
281 classes had all the genes necessary for CO₂-fixation to pyruvate via the reductive glycine pathway²¹
282 (Figs. 4 & 5). Of the residual nine DPO MAGs whose reductive glycine pathway was incomplete,
283 four were missing homologs of serine deaminases, preventing the final conversion of serine to
284 pyruvate (SI Dataset S6). The remaining five DPO MAGs (ranging from 61.3 – 98.7% completion)
285 were missing between one and four genes involved in formate and/or glycine transformations,
286 severely impeding the overall pathway (SI Datasets S5, S6). It is possible that homologous
287 enzymes may perform the reactions of missing genes, as might be the case for one genome
288 (*Syntrophales* LM1) which harbored a serine-glyoxylate transaminase as opposed to the standard
289 serine deaminase (SI Dataset S6). Even if not a universal carbon fixation pathway in DPOM, our
290 analyses suggest the reductive glycine pathway might be an important autotrophic mechanism
291 across diverse DPO taxa. Carbon-tracing studies will be necessary to understand how individual
292 DPOM use CO₂ to simultaneously generate biomass and capture energy from phosphite oxidation.

293 ***ptx-ptd* Cluster Diversity.** DPO activity in FiPS-3 and Phox-21 was attributed to the *ptx-ptd* gene
294 cluster, and only organisms with *ptx-ptd* genes were enriched, positing this to be the dominant, or
295 possibly sole, metabolic pathway underlying phosphite oxidation^{13,14,17} (Fig. 2A). To determine the
296 prevalence and diversity of DPOM beyond our enrichments, we used the PtxD protein sequence
297 from FiPS-3 as a marker gene to query the IMG/M protein sequence space (SI Dataset S7). We
298 recovered 15 positive hits that were phylogenetically compared to the PtxD from our enriched DPO
299 MAGs and the two previously known DPO species (Fig. 7).

300 Our analysis revealed that the DPO-PtxD form a monophyletic clade that included all validated
301 DPOM (i.e. FiPS-3, Phox-21, and our enriched DPOM). The DPO-PtxD belonged to the
302 glyoxylate/hydroxypyruvate reductase B (GHRB) protein sub-family of the D-2-hydroxyacid
303 dehydrogenases (2HADH). The closest relatives of DPO-PtxD are the sugar dehydrogenases and
304 the PtxD homologs involved in phosphorus assimilation⁴⁰ (Fig. 7A, SI Dataset S8). The DPO PtxD
305 can be distinguished from closely related proteins based on the presence of nearby *ptd* genes (Fig.
306 7). The closest non-DPO homolog (Ga0209611_10199181) of the DPO-PtxD lacks the remaining
307 *ptx-ptd* genes in the inclusion-matrix (Fig. 7C), demonstrating the specificity of our custom pHMMs
308 (File S1 – S7).

309 The DPO PtxD was found exclusively in anoxic environments (Fig. 7B). The predicted failure of
310 DPOM to occupy oxic environments, despite the thermodynamic favorability of DPO coupled to
311 oxygen respiration ($\Delta G^\circ = -283 \text{ kJ.mol}^{-1} \text{ PO}_3^{3-}$), suggests that metabolic proteins may be oxygen
312 sensitive. Alternatively, DPO metabolism may be dependent on the biochemical pathways of
313 anaerobes. While DPOM appear to be common members of diverse anoxic environments, further
314 analyses will be required to describe their relative abundance in natural habitats.

315 **Evolutionary History.** The DPO evolutionary history was ascertained using (i) genomic features
316 (ii) comparative taxonomic clustering, and (iii) syntenic conservation. Within the DPO-PtxD clade,
317 proteins clustered based on host taxonomy, and the PtxD was distinguishable at the genus level
318 (Fig. 7B). The only deviation from this pattern was *Ca. Smithella phosphorovis* LM1 of the
319 *Syntrophia* class, which had a PtxD lineage consistent with *Ca. Phosphitivorax* species of the
320 *Desulfomonilia_A* class (Fig. 7B). The *ptx-ptd* cluster from *Ca. S. phosphorovis* LM1 occurred on a
321 single contig (13,378 bp) that hosted an IS91 family transposase. This contig had a sequencing
322 depth (64.7x) three-fold that of the bin's average coverage (19.4x), and the GC content (57.4%)
323 was 3.5% higher than the host genome mean GC content (53.9%). Together these findings suggest
324 that, like FiPS-3¹⁶, *Ca. S. phosphorovis* LM1 likely acquired its *ptx-ptd* genes through horizontal
325 gene transfer (HGT). Consistent with this conclusion, the LM1 community assembly did not include
326 taxonomic marker genes for *Ca. Phosphitivorax* species, and the assembly graph supported the
327 binning results, precluding a different bin-assignment for this contig.

328 In contrast to FiPS-3 and *Ca. S. phosphorovis* LM1, most PtxD clustered according to host
329 taxonomy, indicating that most DPOM likely acquired their PtxD via vertical inheritance (Fig. 7B).
330 Similar taxonomic clustering occurred for the PtdC and PtdF, further suggesting that the *ptx-ptd*
331 genes are inherited as a metabolic unit (SI Fig. S3). Tanglegram analyses facilitate a coarse
332 approximation of topological similarity between gene phylogenies, where crossing lines (“tangles”)
333 indicate alternative evolutionary histories⁴¹. Comparisons of the PtxD, PtdC, and PtdF exhibited
334 zero tangling, supporting a linked evolutionary history (SI Fig. S4). Although the phylogenetic trees
335 of individual DPO genes showed alternative branching patterns, this was expected, as genes with
336 functional differences are subject to unique selective pressures.

337 Synteny provides an alternative metric to gauge the unison of *ptx-ptd* gene evolution because: (i)
338 linked genes tend to maintain organization throughout evolutionary history, and (ii) closely related
339 taxa show high genomic stability^{42,43}. We found that the individual *ptx* and *ptd* genes were always
340 codirectional in the order *ptxED* and *ptdCF(G)HI*, respectively (SI Fig. S5). However, the
341 directionality between the *ptx* and *ptd* gene clusters was variable and syntenic variation formed
342 four distinct groups (Groups I-IV, SI Fig. S5) that correlated with host taxonomy. Groups I and IV
343 do not contain *ptdG*, suggesting it is nonessential (SI Fig. S5). While other genes were frequently
344 missing from the *ptx-ptd* cluster, synteny analysis suggested this is due to fragmented contigs (Fig.
345 6C, SI Fig. S5). For example, *Synergistaceae* SL3 was identified as a DPOM in our enrichments,
346 but our pHMM search failed to identify its PtxD (Fig. 7). Synteny suggested that the PtxD was
347 truncated downstream of PtxE, which was confirmed by BLAST alignment (SI Fig. S5).

348 Searching metagenome databases with additional DPO genes would likely reveal other DPO
349 contigs that were split from the PtxD. This was the case when we mined the IMG/M database for

350 PtdC and identified five additional contigs with divergent PtxD phylogeny (Fig. 6A, SI Fig. S4). While
351 these divergent genes may indicate further DPO diversity, their contigs showed non-canonical *ptx-*
352 *ptd* neighborhoods and are not yet represented by validated DPO cultures. For those *ptx-ptd*
353 clusters that confidently represent DPOM, the predominance of vertical transfer was collectively
354 supported by genomic features, taxonomy, and synteny.

355 Discussion

356
357 We used cultivation-based investigations coupled to high-resolution metagenomics to clarify many
358 of the confounding factors that have precluded understanding of DPO. Results from our studies
359 have expanded the known diversity of DPOM ten-fold (from 2 to 21 genomes). Notably, phosphite
360 oxidation coupled to CO₂ reduction appears to be the primary metabolic niche occupied by DPOM.
361 Although DPO coupled to any known inorganic electron acceptor (oxygen, manganese,
362 perchlorate, nitrate, iron, sulfate etc.) is thermodynamically favorable, DPOM genomes encode
363 sparse electron transport machinery and are largely devoid of the enzymes required to reduce
364 these compounds. CO₂ was the only exogenous electron acceptor provided to our sequenced
365 enrichments, and physiological experiments demonstrated a CO₂-dependency. Yet DPOM also
366 lacked canonical carbon reduction or fixation pathways. The reductive glycine pathway was present
367 in many DPOM and may support CO₂ fixation, but the method by which CO₂ is fixed by the
368 remaining DPOM is unknown, as is the end product of CO₂ reduction (e.g. ethanol or lactate),
369 begging future metabolomic analyses.

370 The highly specialized metabolic repertoire of DPOM is analogous to that of syntrophs,
371 corroborating the observation that DPOM frequently belong to known syntrophic taxa⁴⁴.
372 Thermodynamically, phosphite is too energetically favorable an electron donor to require a
373 syntrophic partner, but such a co-dependency would explain their resistance to isolation¹⁷. *D.*
374 *phosphitoxidans* FiPS-3 remains the only cultured isolate to date, yet we failed to cultivate any
375 close relatives of FiPS-3 in our enrichments, despite otherwise representing much of the DPO
376 diversity present in global metagenomes. Furthermore, we found that FiPS-3 is phenotypically and
377 genotypically anomalous when compared to other DPOM. FiPS-3 exhibits greater metabolic
378 versatility than typical DPOM, reducing sulfate, thiosulfate, and nitrate as electron acceptors in
379 addition to CO₂^{13,16,17}. FiPS-3 is also one of only two examples by which the *ptx-ptd* genes were
380 likely acquired via HGT, suggesting that DPO is not its primary energy metabolism. Future efforts
381 to cultivate DPOM may consequently be informed by our DPO MAGs, whose metabolic features
382 suggest a dependence on limited substrates and a potential requirement for microbial partnerships.

383 Our DPOM spanned six classes of three bacterial phyla (*Desulfobacterota*, *Firmicutes* and
384 *Synergistota*). Such sparse representation across diverse taxa is typically indicative of broad-host-
385 range HGT, but phylogenetic analyses of the *ptx-ptd* gene cluster showed that DPO metabolic gene
386 evolution mirrored the host taxonomy. This indicates that vertical transfer is the predominant
387 mechanism of inheritance. Small variations in synteny further support the correlation between gene
388 order and taxonomy while also suggesting that *ptx-ptd* genes have coevolved as a metabolic unit
389 specialized for DPO metabolism.

390 Given the diversity of DPOM lineages that likely inherited the *ptx-ptd* gene cluster vertically, it is
391 tempting to speculate the biological timescale for when DPO metabolism originated. The last
392 common node for all known DPOM suggests that DPOM arose before the divergence of monoderm
393 and diderm bacteria⁴⁵. Mapping the divergence of these clades to geological timescales suggests
394 that DPOM ~3.2 Gya⁴⁶, contemporaneously with anoxygenic photosynthesis and ~0.8 Gya after
395 the evolution of methanogenesis⁴⁶. This is consistent with the suggestion that phosphite composed
396 40-67% of dissolved phosphorus species in Archaean oceans (>3.5 Gya)^{47,48}. The half-life of
397 oceanic phosphite under a reducing atmosphere is expected to be 0.1-10 billion years, which would
398 have allowed phosphite persistence on early Earth, possibly supporting a robust
399 chemolithoautotrophic DPO population.

400 One would expect such an ancient metabolism to be detected more broadly across all bacteria.
401 However, oxygenation of Earth's atmosphere since the great oxidation event (~2.5 Gya) has likely
402 depleted ancient natural phosphite reserves, as oxidizing radicals abiotically oxidize phosphite on
403 geological timescales^{3,49}. Phosphite would consequently be too rare for DPO in most contemporary
404 environments, and lack of positive selection would promote widespread gene loss⁵⁰. Yet pockets
405 of phosphite (0.1 – 1.3 μ M) exist in diverse contemporary environments, and phosphite oxidizing
406 metabolisms still occur in various habitats on extant Earth^{10,22,51,52}. Environmental metadata from
407 global metagenomes identified DPOM in multiple anoxic environments that represent relics of
408 ancient Earth (i.e. oil reservoirs, deep subsurface aquifers) and serve as potential examples of
409 contemporary phosphite accumulation (i.e. wastewater sludge, freshwater wetlands). A number of
410 environments evidently continue to support phosphorus redox cycling. By coupling DPO to primary
411 production via an uncharacterized CO₂ reduction pathway, DPOM likely play a unique ecological
412 role in any environment they inhabit.

413 **Methods**

414

415 **Growth Conditions and Sampling.**

416 Enrichment inocula were obtained from six wastewater treatment facilities in the San Francisco
417 Bay area of California (SI Dataset S1). Serum bottles (150ml volume) (Bellco, Vineland, NJ, USA)
418 containing basal media (45mL) were each inoculated with sludge (5mL) and incubated at 37 °C.
419 Anoxic medium was prepared by boiling under N₂/CO₂ (80:20, v/v) to remove dissolved O₂, and
420 dispensed under N₂/CO₂ (80:20, v/v) into anaerobic pressure tubes or serum bottles. These were
421 capped with thick butyl rubber stoppers and sterilized by autoclaving (15 min at 121 °C). The basal
422 medium was composed of (per 1 L of DI water): 5 g NaHCO₃, 12 g HEPES buffer, 1 g NH₄Cl, 0.5
423 g KCl, 1.5 g MgCl₂, 0.15 g CaCl₂ (2H₂O), 0.5 g L-cysteine HCl and 10 mL each of vitamins and
424 trace minerals⁵³. Saline medium additionally contained 20 g/L NaCl. Salt solutions of Na₂HPO₃,
425 Na₂SO₄, and NaNO₃ (10mM) were added from sterile anoxic stocks as needed. Rumen fluid (Bar
426 Diamond Inc, Parma, ID, USA), prepared by degassing (30 minutes with N₂) and autoclaving (121
427 °C for 30 min), was added to the basal media as required. Heat killed controls were autoclaved at
428 121 °C for 1 h. Samples for DNA extraction were pelleted by 30 min centrifugation at 10,000 rcf
429 and stored at -80 °C. Samples for ion determination were filtered and stored at 4 °C prior to ion
430 chromatography (IC) using the method described previously¹⁷. Cell growth was measured as
431 optical density at 600nm (OD₆₀₀) using a Genesys™ 20 Visible Spectrophotometer (Thermo
432 Scientific).

433

434 **Metagenomic Assembly, Binning, and Annotation.**

435 Sequenced communities were grown in triplicate cultures amended with 5% rumen fluid with or
436 without 10 mM phosphite (SI Fig. S1). DNA was extracted from the no-phosphite triplicates in
437 stationary phase (-Ps), and the 10 mM phosphite triplicates in exponential phase (+Pe) and
438 stationary phase (+Ps) (SI Fig. S1). Community R1 failed to reach stationary phase and was only
439 represented by samples -Ps and +Pe. Communities LM1, R3, SL1, and SL3 failed to reproduce
440 activity and were instead sampled from two previously active enrichments (E1 and E2) (SI Fig. S1).
441 DNA was extracted using the DNeasy PowerLyzer Microbial Kit (Qiagen) and sequenced with an
442 Illumina HiSeq 4000 (150 bp paired-end reads) at the UC Berkeley Vincent J. Coates Genomics
443 Sequencing Laboratory. Reads were trimmed and filtered using Sickle v1.33 (quality threshold
444 value of 20)⁵⁴. Gene-level taxonomy was assigned using Centrifuge v1.0.1-beta-27-g30e3f06ec3
445 ⁵⁵. Reads for each of the 11 communities were combined and co-assembled using MEGAHIT v1.1.2
446 ⁵⁶ using the meta-sensitive preset. Reads were mapped to assembled contigs using BWA-MEM
447 v0.7.17 ⁵⁷ with default parameters. Contigs over 1000 bp from each combined assembly were
448 binned into individual genomes using Anvi'o v5.4.0 ⁵⁸. Communities with < 30,000 contigs (LM3,
449 M1, R1, SM1, SM3, SV1, SV3) were binned manually using patterns of hierarchical clustering,
450 sequencing coverage, GC content, and gene-level taxonomic assignments. Communities with >

451 30,000 contigs (LM1, R3, SL1, SL3) were binned automatically using CONCOCT then manually
452 refined with the Anvi'o graphical interface⁵⁹. Quality of metagenome-assembled genomes (MAGs)
453 was measured from lineage-specific, conserved, single-copy marker genes using the CheckM
454 v1.0.18 lineage workflow⁶⁰. The resulting 11 co-assemblies consisted of 1900 Mbp, 1.99 million
455 contigs, and 574 draft genomes (SI Dataset S2). Only draft genomes of medium quality or greater
456 (>50% completion; <10% redundant)²⁴ were subjected to further study, resulting in 239
457 metagenome-assembled genomes (MAGs) that represent 60% (647 Mbp) of the binned contigs (SI
458 Dataset S3). Open reading frames were predicted from selected genomes using Prodigal v2.6.3⁶¹
459 and assigned taxonomy using the Genome Taxonomy Database toolkit (GTDB-Tk)²⁶, which placed
460 MAGs into protein reference trees using concatenated SCG sets. Contigs of interest were
461 functionally annotated with Prokka v1.14.6⁶².

462 The DPO MAGs were also annotated with DRAM⁶³, a genome annotation tool that provides
463 metabolic profiles for each input genome. For contigs of interest, these annotations were compared
464 to Prokka v1.14.6 annotations⁶². More detailed DRAM analyses are provided in Shaffer & Borton
465 *et al.*⁶³. The raw annotations containing an inventory of all database annotations for every gene
466 from each input genome are reported in SI S6. From the raw annotations, DRAM then summarizes
467 key metabolisms across the genomes, with SI Figure S2 showing the DRAM Product output. All
468 code for DRAM is available on github: <https://github.com/shafferm/DRAM>.

469 **Identification of Metagenomic DPO Proteins.**

470 DPO proteins (PtxD, PtdC, PtdF) were identified from publicly available metagenomes. The largest
471 metagenomes (representing 90% of proteins from each ecosystem category) in the JGI Integrated
472 Microbial Genomes and Metagenomes (IMG/M) database were collected (n=17,888) on August 1,
473 2018 (SI Dataset S7). Sequence data from the IMG/M database were produced by the US
474 Department of Energy Joint Genome Institute (<http://www.jgi.doe.gov/>) in collaboration with the
475 user community. The FiPS-3 PtxD, PtdC, and PtdF were searched against all proteins using
476 BLASTP with bit score thresholds of 270, 300, and 250 respectively. Positive hits were aligned
477 using MUSCLE v3.8.1551⁶⁴ and constructed into an approximately maximum-likelihood
478 phylogenetic tree using FastTree v2.1.11⁶⁵ with 1000 bootstrap resamplings. DPO proteins were
479 defined as (i) those that formed a phylogenetically distinct clade with proteins from experimentally
480 validated DPOM (ii) were found on a contig near at least one other putative DPO gene and (iii)
481 were at least 90% the length of their homolog protein in FiPS-3. Protein sequences from the
482 identified *ptx-ptd* gene clusters were used to create profile Hidden Markov Models (pHMMs) for
483 each of the PtxDE-PtdCFGHI proteins using HMMER v3.2.1^{66,67}. These pHMMs are available as
484 supplementary files (SI Files S1-S7). Bit score thresholds for stringent *de novo* identification of
485 DPO proteins were determined by a reciprocal pHMM search on a subset of the IMG/M database
486 (SI Dataset S9). To compare the evolutionary relationships between the PtxD, PtdC, and PtdF,
487 members of the DPO clade were dereplicated with CD-HIT v4.8.1⁶⁸ by clustering proteins with
488 100% sequence similarity and selecting the largest contig to represent each gene cluster in a
489 simplified phylogenetic tree. Tanglegrams comparing PtxD to PtdC and PtdF were generated with
490 Dendroscope v3.7.2⁶⁹. Gene synteny was visualized with SimpleSynteny⁷⁰, where genes were
491 identified with BLAST and annotated according to our custom pHMMs.

492 **Characterization of DPO Genomes.**

493 Annotated proteins from all MAGs were searched for known DPO genes (*ptxDE-ptdCFGHI*) with
494 our custom pHMMs. MAGs were operationally considered capable of DPO if they included at least
495 one gene from the *ptx-ptd* gene cluster. The *ptx-ptd* genes that were absent from MAGs were
496 searched for in all remaining contigs of the respective community.

497 A pHMM for the rpS8 was obtained from Wu *et al.* and applied to all DPO MAGs^{67,71}. The rpS8
498 gene has been shown to effectively represent whole-genome average nucleotide identity (ANI)
499 values²⁷ and was present once in each DPO MAG. Each rpS8 was BLAST searched against the

500 NCBI GenBank database to identify the closest relative, closest isolated relative, and informative
501 representatives for phylogenetic analysis. Identified close relatives corresponded to the multi-gene
502 taxonomy assignments of the GTDB (SI Dataset S4). Sequences were aligned using MUSCLE
503 v3.8.1551⁶⁴, and an approximately-maximum-likelihood phylogenetic tree was constructed with
504 1000 bootstrap resamplings using FastTree v2.1.11⁶⁹. Trees were visualized using FigTree v1.4.4
505 (<http://tree.bio.ed.ac.uk/software/figtree/>).

506 The 16S rRNA gene for each community was reconstructed from metagenomic reads using default
507 parameters in EMIRGE with 50 iterations²⁵. Reconstructed genes were classified using SILVA³⁵
508 and mapped back to the 16S rRNA gene fragments of DPO MAGs. The novelty of each DPO MAG
509 was determined by the rank of closest relatives in the GTDB, NCBI (rpS8), and SILVA (16S rRNA
510 gene) databases (SI Dataset S4). A DPO MAG was considered novel at the specified rank (i.e.
511 species, genus) based on the following thresholds: (i) GTDB, considered novel if there were no
512 logged relatives for that rank; (ii) NCBI (rpS8), considered a novel species if the closest relative
513 was <98.3% identity; (iii) SILVA (16S rRNA gene) considered a novel species if the closest relative
514 shared <96.7% identity and a novel genus if the closest relative shared <94% identity²⁷. The novelty
515 of a DPO MAG was assigned based on the lowest resolved taxonomic rank between all searched
516 databases.

517 Data Deposition

518 All metagenomic reads, assemblies, and curated metagenome-assembled genomes (MAGs;
519 quality metrics >50% complete and <10% redundant) are available through the NCBI BioProject
520 accession PRJNA655520.

521 Acknowledgments

522
523 We thank A. Englebretson, I. Figueroa, M. Silverberg, Y. Liu, C. Thrash, J. Taylor, and S. McDevitt
524 for laboratory support and guidance on evolutionary analysis and sequencing. Wastewater sludge
525 samples were generously provided by Judy Walker (San Leandro Water Treatment), Alope Vaid
526 (Veolia Water North America, Richmond), Bob Wandro & Robert Huffstutler (Silicon Valley Clean
527 Water), Jan Guy & Pete Dallabetta (San Mateo Waste Water Treatment Plant), Nimisha Patel
528 (Sewerage Agency of Southern Marin), and Jimmie Truesdell (City of Livermore Water Resources
529 Department). Funding for phosphorus redox cycling is provided by the Energy & Biosciences
530 Institute (Berkeley, CA) and the US Department of Energy Genomic Science Program to J.D.C.
531 through grant number DE-SC0020156. Independent funding to S.D.E through the EBI-Shell
532 Fellowship was supported by Shell International Exploration and Production Inc.
533

534 **Competing Interests.** The authors declare no competing interests.
535

536 References.

- 537 1. Pasek, M. A., Sampson, J. M. & Atlas, Z. Redox chemistry in the phosphorus
538 biogeochemical cycle. *Proc. Natl. Acad. Sci.* **111**, 15468–15473 (2014).
- 539 2. Figueroa, I. A. & Coates, J. D. Microbial Phosphite Oxidation and Its Potential Role in the
540 Global Phosphorus and Carbon Cycles. *Adv. Appl. Microbiol.* **98**, 93–117 (2017).
- 541 3. Pasek, M. A. Rethinking early Earth phosphorus geochemistry. **105**, 853–858 (2008).
- 542 4. Herschy, B. *et al.* Archaean phosphorus liberation induced by iron redox geochemistry.
543 *Nat. Commun.* 1–7 (2018) doi:10.1038/s41467-018-03835-3.
- 544 5. Britvin, S. N., Murashko, M. N., Vapnik, Y., Polekhovskiy, Y. S. & Krivovichev, S. V. Earth's
545 phosphides in Levant and insights into the source of Archaean prebiotic phosphorus. *Sci.*
546 *Rep.* **5**, 10–14 (2015).
- 547 6. Han, C. *et al.* Phosphite in sedimentary interstitial water of Lake Taihu, a large eutrophic

- 548 shallow lake in China. *Environ. Sci. Technol.* **47**, 5679–5685 (2013).
- 549 7. White, A. K. & Metcalf, W. W. The htx and ptx Operons of *Pseudomonas stutzeri* WM88
550 Are New Members of the Pho Regulon. *J. Bacteriol.* **186**, 5876–5882 (2004).
- 551 8. Costas, A. M. G., White, A. K. & Metcalf, W. W. Purification and Characterization of a
552 Novel Phosphorus-oxidizing Enzyme from *Pseudomonas stutzeri* WM88. *J. Biol. Chem.*
553 **276**, 17429–17436 (2001).
- 554 9. Wilson, M. M. & Metcalf, W. W. Genetic Diversity and Horizontal Transfer of Genes
555 Involved in Oxidation of Reduced Phosphorus Compounds by *Alcaligenes faecalis*
556 WM2072. *Appl. Environ. Microbiol.* **71**, 290–296 (2005).
- 557 10. White, A. K. & Metcalf, W. W. Microbial Metabolism of Reduced Phosphorus Compounds.
558 *Annu. Rev. Microbiol.* **61**, 379–400 (2007).
- 559 11. Roels, J. & Verstraete, W. Biological formation of volatile phosphorus compounds.
560 *Bioresour. Technol.* **79**, 243–250 (2001).
- 561 12. Schink, B. & Friedrich, M. Bacterial metabolism: Phosphite oxidation by sulphate
562 reduction. *Nature* **406**, 37 (2000).
- 563 13. Poehlein, A., Daniel, R., Schink, B. & Simeonova, D. D. Life based on phosphite: a
564 genome-guided analysis of *Desulfotignum phosphitoxidans*. *BMC Genomics* **14**, 753
565 (2013).
- 566 14. Simeonova, D. D., Susnea, I., Moise, A., Schink, B. & Przybylski, M. “Unknown Genome”
567 Proteomics. *Mol. Cell. Proteomics* 122–131 (2009) doi:10.1074/mcp.M800242-MCP200.
- 568 15. Simeonova, D. D., Wilson, M. M., Metcalf, W. W. & Schink, B. Identification and
569 heterologous expression of genes involved in anaerobic dissimilatory phosphite oxidation
570 by *Desulfotignum phosphitoxidans*. *J. Bacteriol.* **192**, 5237–5244 (2010).
- 571 16. Schink, B., Thiemann, V., Laue, H. & Friedrich, M. W. *Desulfotignum phosphitoxidans* sp.
572 nov., a new marine sulfate reducer that oxidizes phosphite to phosphate. *Arch. Microbiol.*
573 **177**, 381–391 (2002).
- 574 17. Figueroa, I. A. *et al.* Metagenomics-guided analysis of microbial chemolithoautotrophic
575 phosphite oxidation yields evidence of a seventh natural CO₂ fixation pathway. *Proc. Natl.*
576 *Acad. Sci.* 201715549 (2017) doi:10.1073/pnas.1715549114.
- 577 18. Hao, L. *et al.* Novel syntrophic bacteria in full-scale anaerobic digesters revealed by
578 genome-centric metatranscriptomics. *ISME J.* (2020) doi:10.1038/s41396-019-0571-0.
- 579 19. Yishai, O., Bouzon, M., Döring, V. & Bar-Even, A. In vivo assimilation of one-carbon via a
580 synthetic reductive glycine pathway in *Escherichia coli*. *ACS Synth. Biol.* (2018)
581 doi:10.1021/acssynbio.8b00131.
- 582 20. Bar-Even, A. Formate Assimilation: The Metabolic Architecture of Natural and Synthetic
583 Pathways. *Biochemistry* (2016) doi:10.1021/acs.biochem.6b00495.
- 584 21. Sánchez-Andrea, I. *et al.* The reductive glycine pathway allows autotrophic growth of
585 *Desulfovibrio desulfuricans*. *Nat. Commun.* 1–12 (2020) doi:10.1038/s41467-020-18906-7.
- 586 22. Yu, X., Geng, J., Ren, H., Chao, H. & Qiu, H. Determination of phosphite in a full-scale
587 municipal wastewater treatment plant. *Environ. Sci. Process. Impacts* **17**, 441–447 (2015).
- 588 23. Liang, S. *et al.* One-Step Treatment of Phosphite-Laden Wastewater: A Single
589 Electrochemical Reactor Integrating Superoxide Radical-Induced Oxidation and
590 Electrocoagulation. *Environ. Sci. Technol.* **53**, 5328–5336 (2019).
- 591 24. Bowers, R. M. *et al.* Minimum information about a single amplified genome (MISAG) and a
592 metagenome-assembled genome (MIMAG) of bacteria and archaea. *Nat. Biotechnol.* **35**,

- 593 725–731 (2017).
- 594 25. Miller, C. S., Baker, B. J., Thomas, B. C., Singer, S. W. & Banfield, J. F. EMIRGE:
595 Reconstruction of full-length ribosomal genes from microbial community short read
596 sequencing data. *Genome Biol.* **12**, (2011).
- 597 26. Chaumeil, P.-A., Mussig, A. J., Hugenholtz, P. & Parks, D. H. GTDB-Tk: a toolkit to
598 classify genomes with the Genome Taxonomy Database. *Bioinformatics* 1–3 (2019)
599 doi:10.1093/bioinformatics/btz848.
- 600 27. Olm, M. R. *et al.* Consistent Metagenome-Derived Metrics Verify and Delineate Bacterial
601 Species Boundaries. *mSystems* **5**, e00731-19 (2020).
- 602 28. Galushko, A. & Kuever, J. Desulfomonile. in *Bergey's Manual of Systematics of Archaea
603 and Bacteria* (2019).
- 604 29. Kim, A. D., Mandelco, L., Tanner, R. S., Woese, C. R. & Suflita, J. M. Desulfomonile
605 tiedjei gen. nov. and sp. nov., a novel anaerobic, dehalogenating, sulfate-reducing
606 bacterium. *Arch. Microbiol.* **154**, 23–30 (1990).
- 607 30. Rainey, F. A. Pelotomaculum. in *Bergey's Manual of Systematics of Archaea and Bacteria
608* 1–6 (2009).
- 609 31. Imachi, H. *et al.* Pelotomaculum thermopropionicum gen. nov., sp. nov., an anaerobic,
610 thermophilic, syntrophic propionate-oxidizing bacterium. *Int. J. Syst. Evol. Microbiol.* **52**,
611 1729–1735 (2002).
- 612 32. Liu, Y., Balkwill, D. L., Henry, C. A., Drake, G. R. & Boone, D. R. Characterization of the
613 anaerobic propionate-degrading syntrophs *Smithella propionica*. *Int. J. Syst. Bacteriol.* **49**,
614 545–556 (1999).
- 615 33. McInerney, M. J. *et al.* Physiology, ecology, phylogeny, and genomics of microorganisms
616 capable of syntrophic metabolism. *Ann. N. Y. Acad. Sci.* **1125**, 58–72 (2008).
- 617 34. Mouttaki, H., Nanny, M. A. & McInerney, M. J. Cyclohexane carboxylate and benzoate
618 formation from crotonate in *Syntrophus aciditrophicus*. *Appl. Environ. Microbiol.* **73**, 930–
619 938 (2007).
- 620 35. Pruesse, E. *et al.* SILVA: A comprehensive online resource for quality checked and
621 aligned ribosomal RNA sequence data compatible with ARB. *Nucleic Acids Res.* **35**,
622 7188–7196 (2007).
- 623 36. Friedrich, T., Dekovic, D. K. & Burschel, S. Assembly of the *Escherichia coli*
624 NADH:ubiquinone oxidoreductase (respiratory complex I). *Biochim. Biophys. Acta -
625 Bioenerg.* **1857**, 214–223 (2016).
- 626 37. Young, T. *et al.* Crystallographic and kinetic analyses of the FdsBG subcomplex of the
627 cytosolic formate dehydrogenase FdsABG from *Cupriavidus necator*. *J. Biol. Chem.* **295**,
628 6570–6585 (2020).
- 629 38. Jouanneau, Y., Jeong, H. S., Hugo, N., Meyer, C. & Willison, J. C. Overexpression in
630 *Escherichia coli* of the rnf genes from *Rhodobacter capsulatus* - Characterization of two
631 membrane-bound iron-sulfur proteins. *Eur. J. Biochem.* **251**, 54–64 (1998).
- 632 39. Bar-Even, A., Noor, E. & Milo, R. A survey of carbon fixation pathways through a
633 quantitative lens. *J. Exp. Bot.* **63**, 2325–2342 (2012).
- 634 40. Matelska, D. *et al.* Classification, substrate specificity and structural features of D-2-
635 hydroxyacid dehydrogenases: 2HADH knowledgebase. *BMC Evol. Biol.* **18**, 1–23 (2018).
- 636 41. Gordon, B. R. *et al.* Decoupled genomic elements and the evolution of partner quality in
637 nitrogen-fixing rhizobia. *Ecol. Evol.* **6**, 1317–1327 (2016).

- 638 42. Junier, I. & Rivoire, O. Synteny in Bacterial Genomes: Inference, Organization and
639 Evolution. (2013).
- 640 43. Sevillya, G. & Snir, S. Synteny footprints provide clearer phylogenetic signal than
641 sequence data for prokaryotic classification. *Mol. Phylogenet. Evol.* **136**, 128–137 (2019).
- 642 44. Mcinerney, M. J., Sieber, J. R. & Gunsalus, R. P. Syntrophy in Anaerobic Global Carbon
643 Cycles. *Curr. Opin. Biotechnol.* **20**, 623–632 (2010).
- 644 45. Raymann, K., Brochier-Armanet, C. & Gribaldo, S. The two-domain tree of life is linked to
645 a new root for the Archaea. *Proc. Natl. Acad. Sci. U. S. A.* **112**, 6670–6675 (2015).
- 646 46. Battistuzzi, F. U., Feijao, A. & Hedges, S. B. A genomic timescale of prokaryote evolution:
647 Insights into the origin of methanogenesis, phototrophy, and the colonization of land. *BMC*
648 *Evol. Biol.* **4**, 1–14 (2004).
- 649 47. Pasek, M. A., Harnmeijer, J. P., Buick, R., Gull, M. & Atlas, Z. Evidence for reactive
650 reduced phosphorus species in the early Archean ocean. *Proc. Natl. Acad. Sci.* **110**,
651 10089–10094 (2013).
- 652 48. Pasek, M. A role for phosphorus redox in emerging and modern biochemistry. *Curr. Opin.*
653 *Chem. Biol.* **49**, 53–58 (2019).
- 654 49. Lyons, T. W., Reinhard, C. T. & Planavsky, N. J. The rise of oxygen in Earth's early ocean
655 and atmosphere. *Nature* **506**, 307–315 (2014).
- 656 50. Wolf, Y. I. & Koonin, E. V. Genome reduction as the dominant mode of evolution.
657 *BioEssays* 829–837 (2013) doi:10.1002/bies.201300037.
- 658 51. Pirim, C. *et al.* Investigation of schreibersite and intrinsic oxidation products from Sikhote-
659 Alin, Seymchan, and Odessa meteorites and Fe₃P and Fe₂NiP synthetic surrogates.
660 *Geochim. Cosmochim. Acta* **140**, 259–274 (2014).
- 661 52. Pasek, M. & Block, K. Lightning-induced reduction of phosphorus oxidation state. *Nat.*
662 *Geosci.* **2**, 553–556 (2009).
- 663 53. Balch, W. E., Fox, G. E., Magrum, L. J., Woese, C. R. & Wolfe, R. S. Methanogens :
664 Reevaluation of a Unique Biological Group. **43**, 260–296 (1979).
- 665 54. Joshi, N. & JN, F. Sickle: A sliding-window, adaptive, quality-based trimming tool for
666 FastQ files (Version 1.33). [*Software*] (2011).
- 667 55. Kim, D., Song, L., Breitwieser, F. P. & Salzberg, S. L. Centrifuge: rapid and accurate
668 classification of metagenomic sequences. *bioRxiv* **26**, 054965 (2016).
- 669 56. Li, D., Liu, C. M., Luo, R., Sadakane, K. & Lam, T. W. MEGAHIT: An ultra-fast single-node
670 solution for large and complex metagenomics assembly via succinct de Bruijn graph.
671 *Bioinformatics* **31**, 1674–1676 (2015).
- 672 57. Li, H. & Durbin, R. Fast and accurate short read alignment with Burrows-Wheeler
673 transform. *Bioinformatics* **25**, 1754–1760 (2009).
- 674 58. Eren, A. M. *et al.* Anvi'o: an advanced analysis and visualization platform for 'omics data.
675 *PeerJ* **3**, (2015).
- 676 59. Alneberg, J. *et al.* Binning metagenomic contigs by coverage and composition. *Nat.*
677 *Methods* **11**, 1144–1146 (2014).
- 678 60. Parks, D. H., Imelfort, M., Skennerton, C. T., Hugenholtz, P. & Tyson, G. W. CheckM :
679 assessing the quality of microbial genomes recovered from isolates , single cells , and
680 metagenomes. *Genome Res.* 1043–1055 (2015) doi:10.1101/gr.186072.114.Freely.
- 681 61. Hyatt, D. *et al.* Prodigal: Prokaryotic gene recognition and translation initiation site

- 682 identification. *BMC Bioinformatics* **11**, (2010).
- 683 62. Seemann, T. Prokka : rapid prokaryotic genome annotation. *Bioinformatics* **30**, 2068–2069
684 (2014).
- 685 63. Shaffer, M. *et al.* DRAM for distilling microbial metabolism to automate the curation of
686 microbiome function. *Nucleic Acids Res.* 1–58 (2020)
687 doi:<https://doi.org/10.1101/2020.06.29.177501>.
- 688 64. Edgar, R. C. MUSCLE: Multiple sequence alignment with high accuracy and high
689 throughput. *Nucleic Acids Res.* **32**, 1792–1797 (2004).
- 690 65. Price, M. N., Dehal, P. S. & Arkin, A. P. FastTree 2 - Approximately Maximum-Likelihood
691 Trees for Large Alignments. *PLoS One* **5**, (2010).
- 692 66. Johnson, L. S., Eddy, S. R. & Portugaly, E. Hidden Markov model speed heuristic and
693 iterative HMM search procedure. *BMC Bioinformatics* (2010).
- 694 67. Yoon, B. Hidden Markov Models and their Applications in Biological Sequence Analysis.
695 402–415 (2009).
- 696 68. Li, W., Fu, L., Niu, B., Wu, S. & Wooley, J. Ultrafast clustering algorithms for metagenomic
697 sequence analysis. *Brief. Bioinform.* **13**, 656–668 (2012).
- 698 69. Huson, D. H. & Scornavacca, C. Dendroscope 3 : An Interactive Tool for Rooted
699 Phylogenetic Trees and Networks. *Syst. Biol.* **61**, 1061–1067 (2012).
- 700 70. Veltri, D., Wight, M. M. & Crouch, J. A. SimpleSynteny: a web-based tool for visualization
701 of microsynteny across multiple species. *Nucleic Acids Res.* **44**, W41–W45 (2016).
- 702 71. Wu, D., Jospin, G. & Eisen, J. A. Systematic Identification of Gene Families for Use as
703 'Markers' for Phylogenetic and Phylogeny-Driven Ecological Studies of Bacteria and
704 Archaea and Their Major Subgroups. *PLoS One* **8**, (2013).
- 705 72. Mendler, K. *et al.* Annotree: Visualization and exploration of a functionally annotated
706 microbial tree of life. *Nucleic Acids Res.* **47**, 4442–4448 (2019).
- 707 73. Kanehisa, M., Sato, Y., Kawashima, M., Furumichi, M. & Tanabe, M. KEGG as a
708 reference resource for gene and protein annotation. *Nucleic Acids Res.* **44**, D457–D462
709 (2016).

710

711 **Figures and Datasets.**

712

713 **Figure 1: DPO Enrichment Activity.** (A) Representative phosphite oxidation by the SM1
714 community. Temporal ion concentrations are shown for live (solid lines) or autoclaved (dashed
715 lines) inoculum. Enrichments were amended with 10 mM phosphite at the spike point. (B) Percent
716 change of measured ions for each enrichment community. Each row represents one community;
717 each column displays the percent-accumulation or consumption of each titled ion. Row labels are
718 colored according to the added electron acceptor (black, CO₂ only; blue, CO₂+SO₄²⁻; green,
719 CO₂+NO₃⁻). A white dotted line denotes 50% consumption of PO₃³⁻. All percentages were calculated
720 from concentration values *prior* to the first spike point. (C) Duration of ion depletion. Horizontal bars
721 show the time frame for metabolic activity of each measured ion. Colors correspond with panel B
722 (red, PO₃³⁻; blue, SO₄²⁻; green, NO₃⁻).

723

724 **Figure 2: Relative Abundance of DPO MAGs.** (A) Relative abundance of MAGs across samples.
725 Each point represents one MAG. Color represents the presence (black) or absence (grey) of any

726 *ptx-ptd* genes. Top panel compares samples from phosphite-amended exponential phase (+Pe) to
727 no-phosphite (-Ps) controls. Bottom panel compares samples from phosphite-amended stationary
728 phase (+Ps) to no-phosphite (-Ps) controls. (B) Relative abundance of MAGs across time. Each
729 subplot represents one community, while each stacked bar represents the community composition
730 of one sample. Colors indicate the dominant (maroon), second dominant (pink) and third dominant
731 (yellow) DPO members, and all remaining community members (grey). Relative abundance was
732 calculated by dividing the mean coverage of a single MAG by the sum of mean coverages for all
733 MAGs in the respective sample.

734

735 **Figure 3: Phylogenetic Trees of DPO MAGs.** A) A phylogenetic tree of bacterial genomes from
736 the GTDB was visualized with AnnoTree⁷². Nodes of the tree represent class-level taxonomy, and
737 those nodes with DPO organisms are highlighted according to the key. B-D) Phylogenetic trees of
738 the *rpS8* marker gene showing the relationship of DPO MAGs to their closest relatives. Panels
739 depict DPO MAGs belonging to the same phyla: B) *Firmicutes*; C) *Synergistota*; D)
740 *Desulfobacterota*. The DPO MAGs from this study are bolded. Colored squares represent their
741 dominance rank from Fig. 2B. Each close relative is annotated with its species name, accession
742 number and genome-source type (isolate vs. MAG), as well as its percent identity to the most
743 closely related DPO MAG from this study. Clades are colored and labeled by taxonomic class.
744 Internal nodes with bootstrap support of >90% are indicated by closed circles and those with
745 support of >70% by open circles. Scale bars: 0.2 change per amino acid residue.

746

747 **Figure 4: Metabolic model of energy conservation by *Desulfomonilia_A* DPOM** (adapted from
748 Figueroa, *et al.*)¹⁷. Dotted lines represent mechanisms that have not been biochemically confirmed.
749 Balanced equations are provided for phosphite oxidation and CO₂ reduction to D-lactate.
750 **Dissimilatory Phosphite Oxidation proteins:** (1) PtdC, phosphite-phosphate antiporter; (2)
751 PtxDE-PtdFHI, putative phosphite dehydrogenase protein complex. **CO₂ Reduction (Reductive
752 Glycine Pathway) proteins:** (3) FdhAB/FdoGHI, formate dehydrogenase; (4) Fhs, formate:THF
753 ligase; (5) FodD, methylene-THF dehydrogenase/methenyl-THF cyclohydrolase; (6) glycine
754 cleavage system (GcvH, lipoyl-carrier protein; GcvPAB, glycine dehydrogenase; GcvT,
755 aminomethyltransferase; Lpd, dihydrolipoyl dehydrogenase); (7) GlyA, serine
756 hydroxymethyltransferase; (8) SdaA/IlvA, serine dehydratase/threonine dehydratase; (9) LdhA, D-
757 lactate dehydrogenase. **Energy Conversion proteins:** (10) ATP synthase complex (11) Rnf,
758 sodium-translocating ferredoxin:NAD oxidoreductase complex (12) NfnAB, NAD-dependent
759 ferredoxin:NADP oxidoreductase.

760

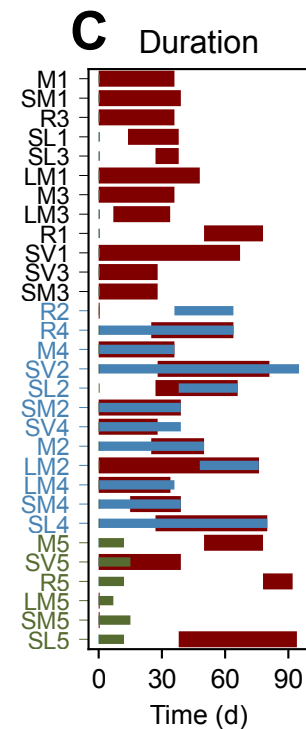
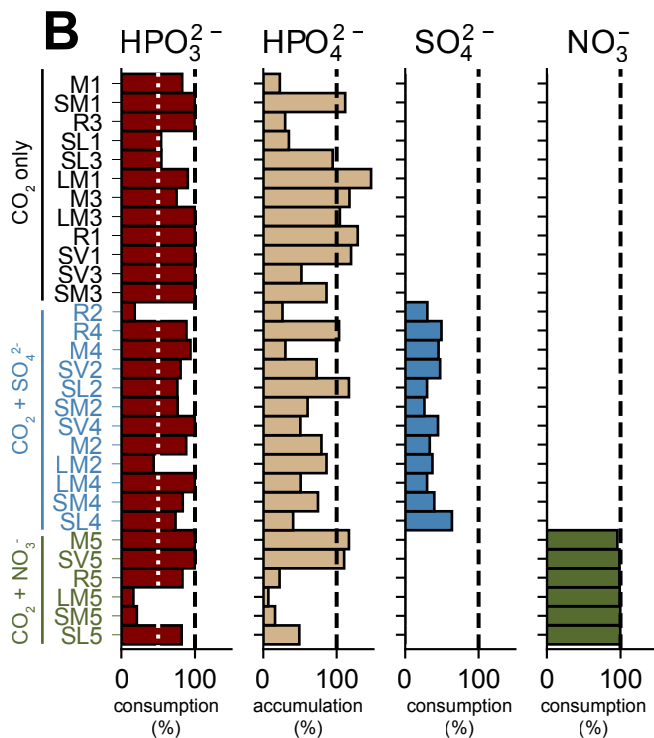
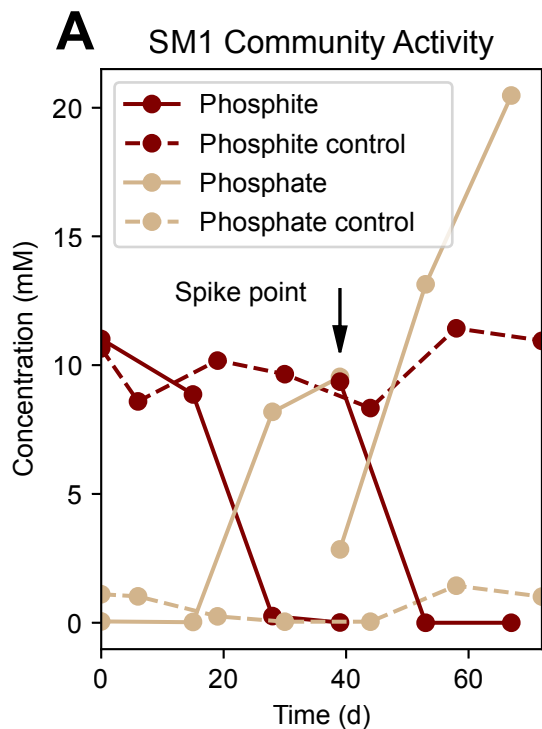
761 **Figure 5: Carbon and Energy Metabolism of DPO MAGs.** Each DPO MAG was subjected to
762 metabolic analysis via DRAM^{63,73}. Within this heatmap, each cell represents a metabolic pathway
763 (columns) for each DPO genome (rows). The number of genes for a given pathway is described by
764 percent completion ranging from 0% (white) to 100% (brown). Pathways are organized into
765 modules related to carbon metabolism, electron transport chain (ETC) complexes, and other
766 enzymes referenced in the text. Organisms are annotated with their taxonomic class.

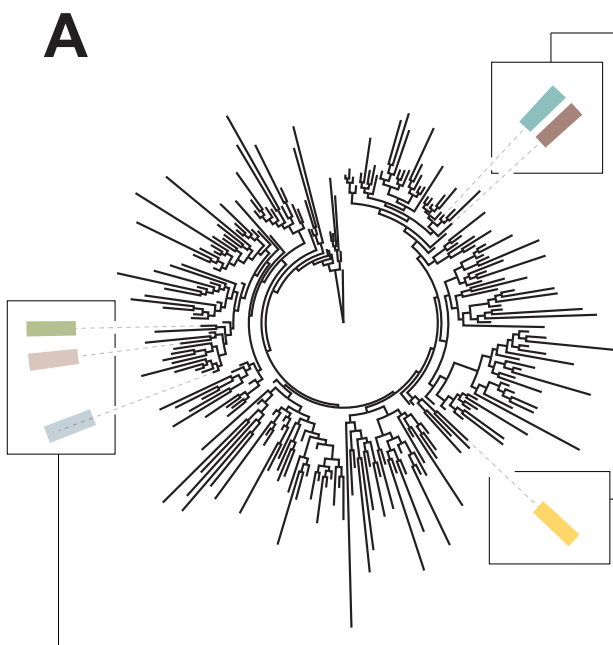
767

768 **Figure 6: CO₂ Dependent DPO Activity.** Growth and phosphite concentrations were temporally
769 monitored in the presence and absence of CO₂ for the SV3 community. Autoclaved controls showed
770 no activity. Error bars represent standard deviation of triplicate cultures.

771

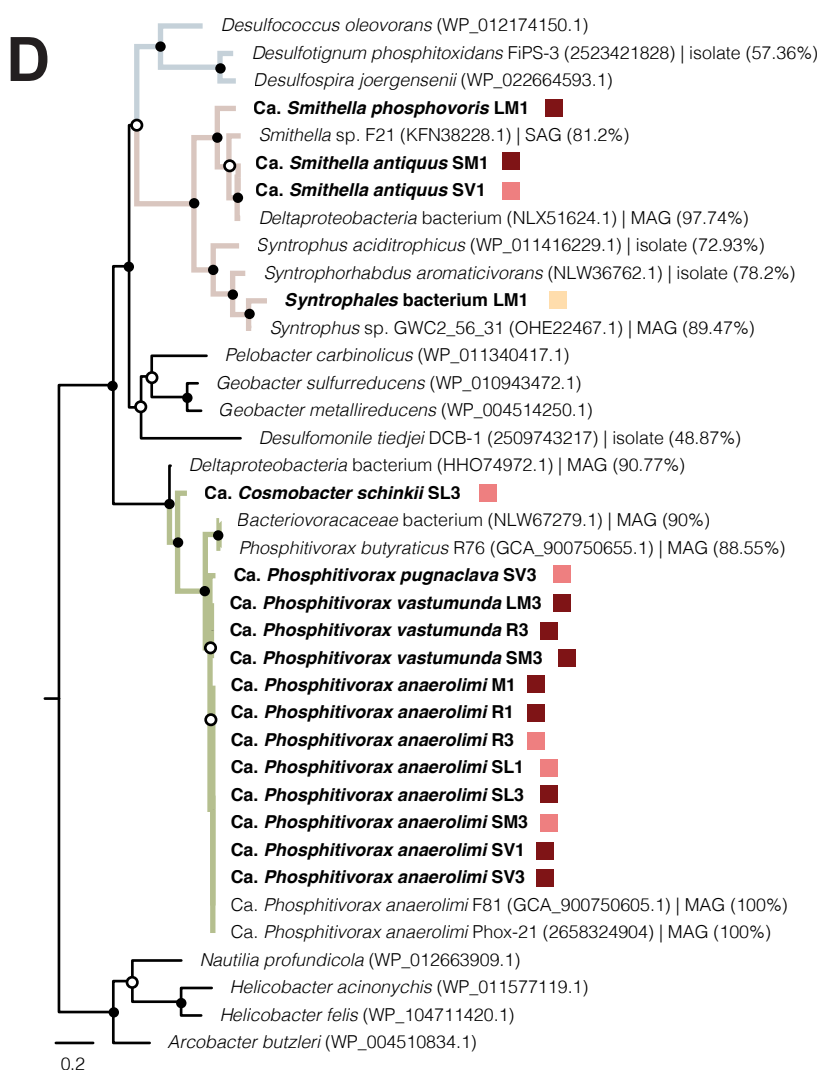
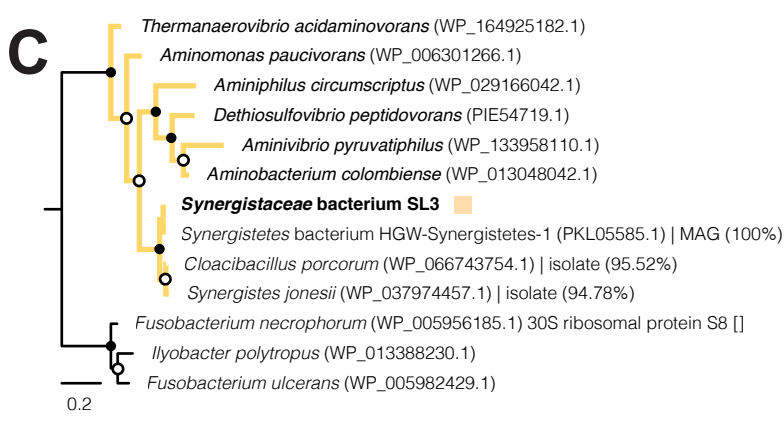
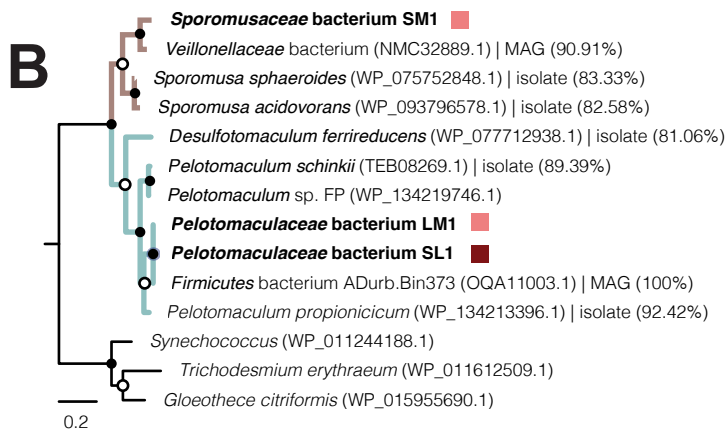
772 **Figure 7: Phylogenetic tree of the phosphite dehydrogenase PtxD.** A) The PtxD from IMG/M
773 metagenomes and DPO MAGs were aligned with proteins from the 2-hydroxyacid dehydrogenase
774 family (Pfam PF00389, set representative proteomes to 15%). Protein subfamilies were assigned
775 based on Matelska et al.⁴⁰. An arrow indicates the location of PtxD proteins that are associated with
776 DPO PtdC but clade with assimilatory phosphite oxidation PtxD (APO). Scale bar: 0.5 change per
777 amino acid residue. B) Refined tree of all PtxD within the DPO-PtxD clade. PtxD from the IMG/M
778 are in light black font and labeled with their source environment and scaffold ID. PtxD from our
779 enriched DPO MAGs are bolded and labeled with their bacterial host name. PtxD that belong to a
780 binned organism are highlighted based on their taxonomic class. Published organisms with
781 validated DPO activity are in red font. Only genes adhering to the IMG/M data usage policy are
782 shown. Internal nodes with bootstrap support of >70% are indicated by closed circles and those
783 with support of >50% by open circles. Scale bar: 0.2 change per amino acid residue. C) The
784 presence (maroon) or absence (light pink) of *ptx-ptd* genes in each genome was determined using
785 custom pHMM models. Genes that were absent from a DPO MAG but present in the assembly are
786 in grey, where phylogeny, tanglegrams, and synteny were collectively used to predict the most
787 likely host. D) Horizontal grey bars display the size (bp) of the contig on which each PtxD was found
788 and are in logarithmic scale to visualize the full range of contig lengths. The black dotted line
789 indicates the minimum length for all seven *ptx-ptd* genes to be present, based on FiPS-3 sequences
790 (7137 bp). Asterisks signify contigs that were binned. bp, base pair.





DPOM Taxonomic Classes by Color

■ <i>Desulfomonilia_A</i>	■ <i>Synergistia</i>
■ <i>Syntrophia</i>	■ <i>Negativicutes</i>
■ <i>Desulfobacteria</i>	■ <i>Desulfotomaculia</i>



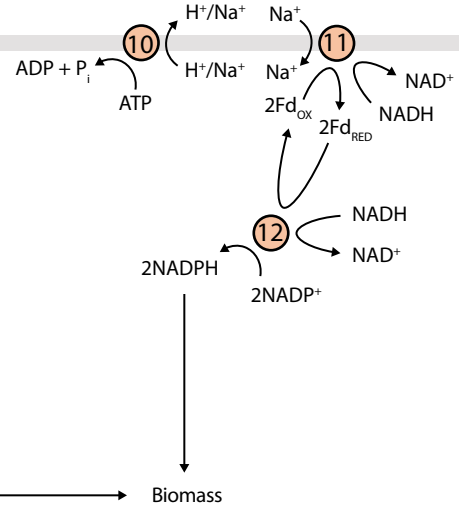
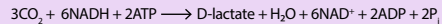
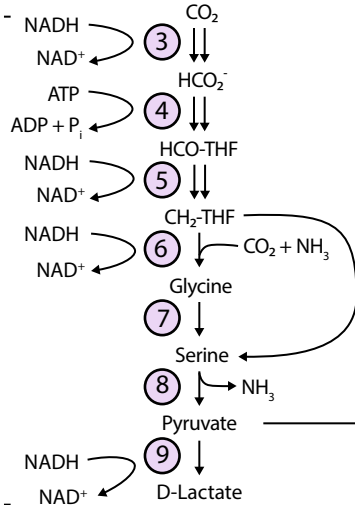
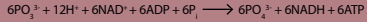
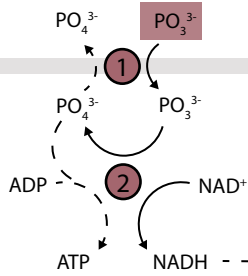
Dissimilatory Phosphite Oxidation

CO₂ Reduction (Reductive Glycine Pathway)

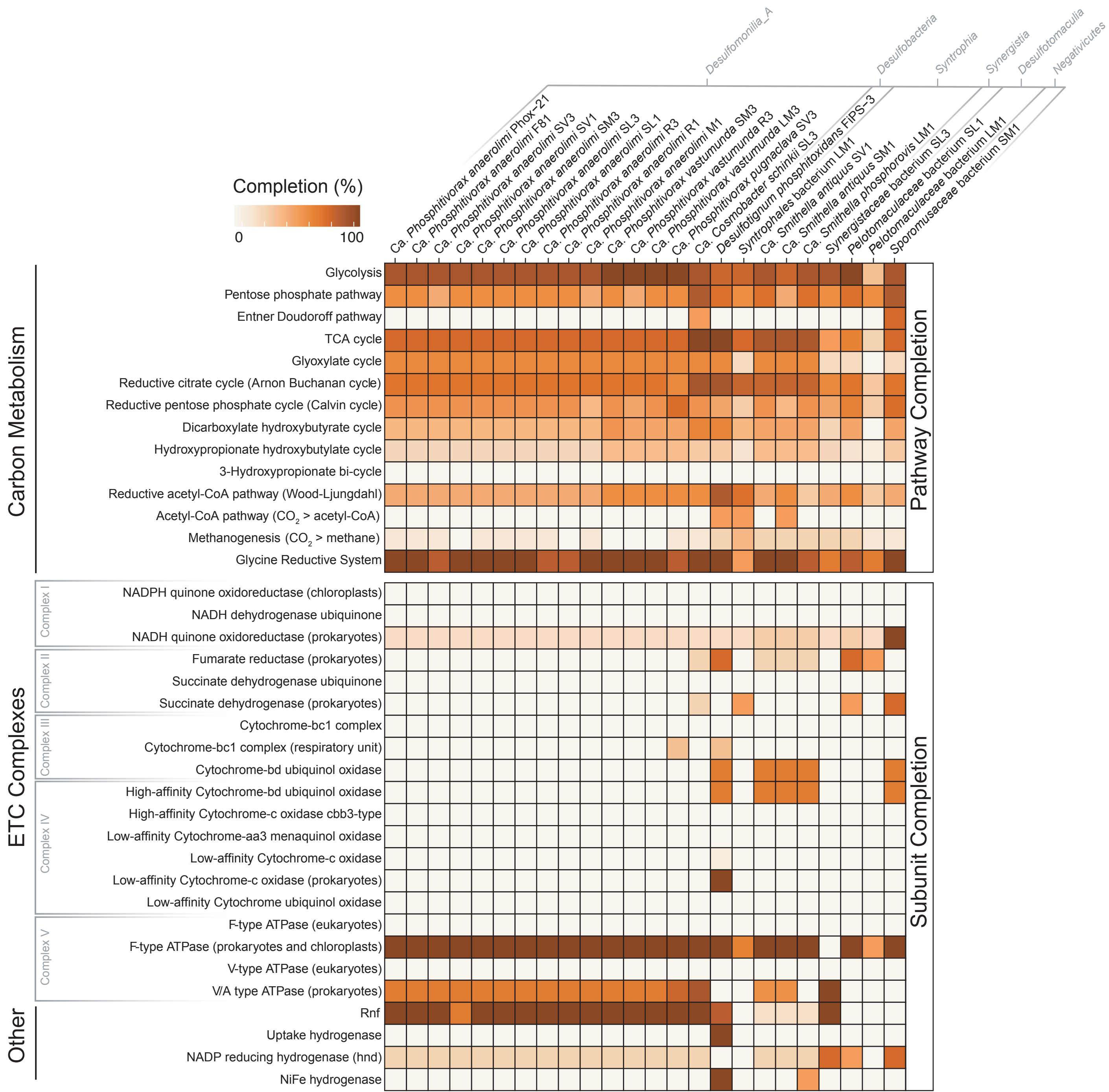
Energy Conversion

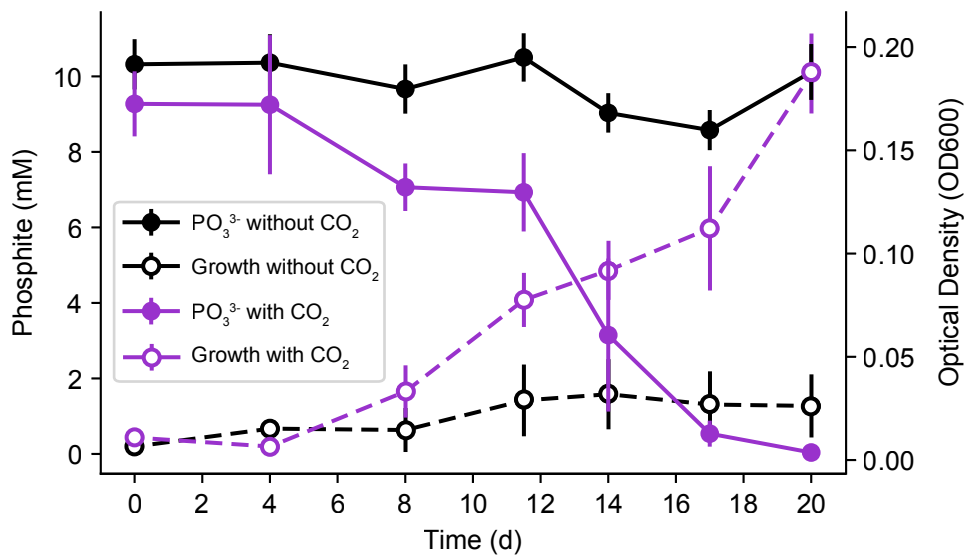
OM

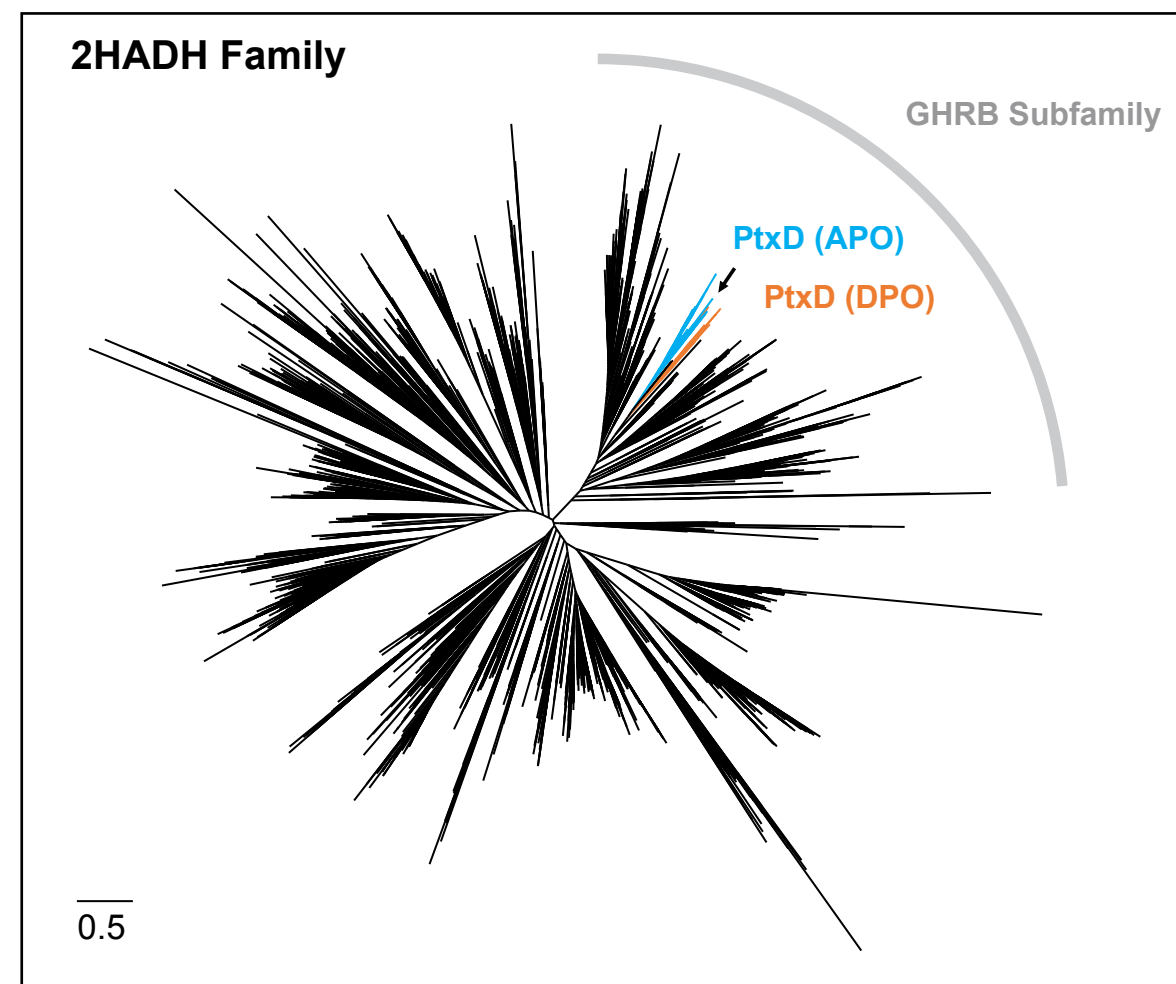
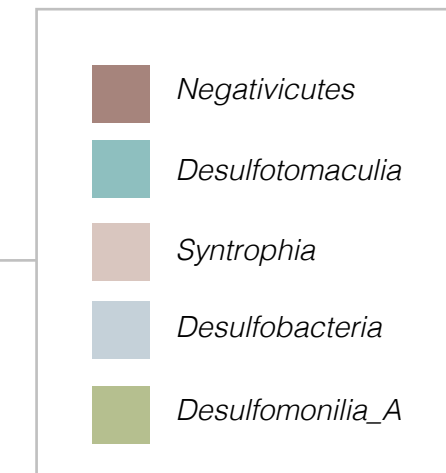
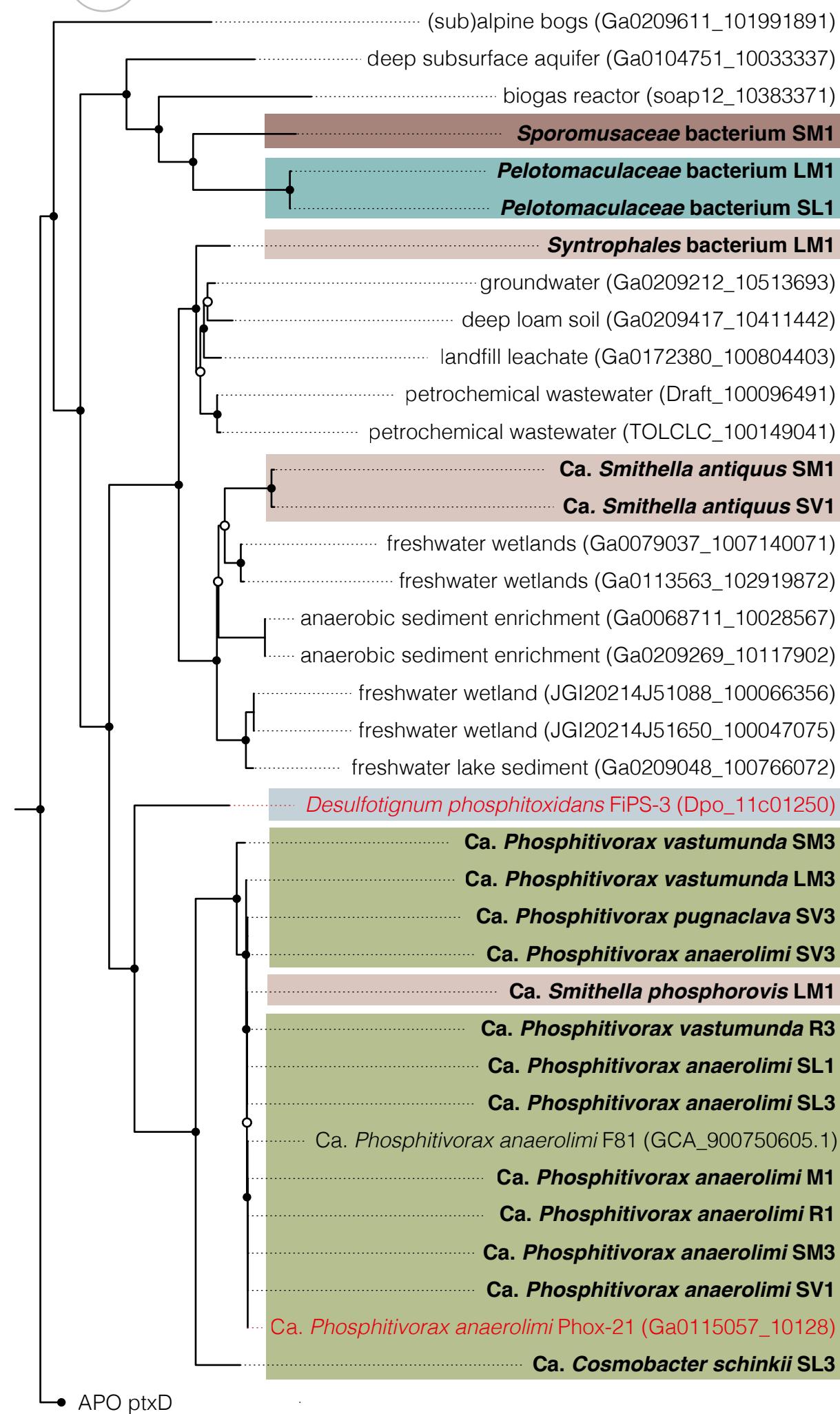
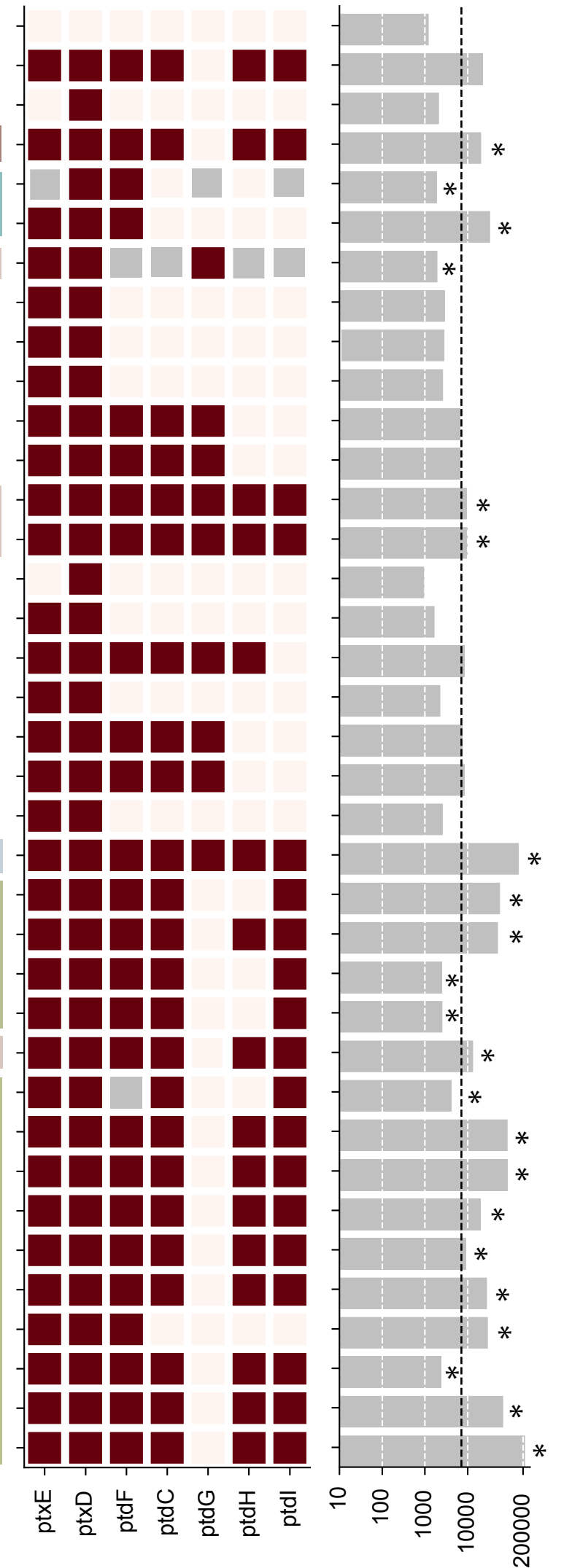
IM



Biomass





A**Panel B Key: Taxonomic Class****B****C***ptx-ptd* genes**D**

scaffold size (bp)

